

2016

ASSESSING THE EFFECT OF SINUS SURGERY ON ORBITAL FRACTURES: IMPLICATIONS FOR PATIENTS WITH RHINOSINUSITIS

Rootu Joshi
rjoshi8@uwo.ca

Follow this and additional works at: <https://ir.lib.uwo.ca/mcap>



Part of the [Anatomy Commons](#)

Citation of this paper:

Joshi, Rootu, "ASSESSING THE EFFECT OF SINUS SURGERY ON ORBITAL FRACTURES: IMPLICATIONS FOR PATIENTS WITH RHINOSINUSITIS" (2016). *Masters of Clinical Anatomy Projects*. 15.
<https://ir.lib.uwo.ca/mcap/15>

ASSESSING THE EFFECT OF SINUS SURGERY ON ORBITAL FRACTURES:
IMPLICATIONS FOR PATIENTS WITH RHINOSINUSITIS

(Project format: Monograph)

by

Rootu Joshi

Graduate Program in Clinical Anatomy

A project submitted in partial fulfillment
of the requirements for the degree of
Master of Science

The School of Graduate and Postdoctoral Studies
The University of Western Ontario
London, Ontario, Canada

© Rootu Joshi 2016

Abstract

Functional endoscopic sinus surgery (FESS), commonly performed to alleviate symptoms of chronic rhinosinusitis, may weaken the thin orbital walls which are susceptible to fracture in facial trauma. This study aims to assess how FESS affects orbital fracture risk. Ten fresh-frozen cadaveric heads underwent FESS on one side. The contralateral side served as intra-specimen control. Orbital trauma was induced using a guided weight-drop technique. Both orbits were tested using sequentially higher drops until orbital fractures were detected on computed tomography scans. Bone mineral density (BMD) was analyzed. All heads presented with a preferential medial wall fracture on the surgical side and orbital floor fracture on the non-surgical side ($p < 0.01$). Reduction in the energy required to induce a fracture in the medial orbital wall post-surgery, and the correlation between BMD and impact energy, was not significant ($p > 0.05$). Results provide improved informed consent for patients with chronic rhinosinusitis.

Keywords

Functional endoscopic sinus surgery, rhinosinusitis, orbital fracture, orbital floor, medial orbital wall, bone mineral density

Co-Authorship Statement

This thesis was written and completed by Rootu Joshi under the supervision of Drs. Marjorie Johnson, Katherine Willmore, Khadry Galil, Thomas Jenkyn, Leigh Sowerby and Corey Moore. The original research question was developed by C. Moore and L. Sowerby. All data collection was performed by R. Joshi and M. Johnson. Analysis and interpretation of data was performed through a collaborative effort between R. Joshi, M. Johnson, K. Willmore and Matthew Harris.

Acknowledgments

I would like to extend my sincerest gratitude to the following individuals for their contributions to this project. This paper could not have been possible without their continued support through the course of my research.

Thank you to Dr. Corey Moore, my primary supervisor, for the conception of this research project, completing physical interventions on cadaveric heads, and for always providing insight and support. Thank you for your mentorship throughout this process and I am grateful to have had the opportunity to work with you.

Thank you to Dr. Marjorie Johnson, my Graduate Affairs Committee member, for her constant support throughout these past two years. Thank you for your assistance in developing my methodology, as well as performing data collection. Your consistent willingness to provide help and encouragement throughout this program has made it one of the most memorable and rewarding experiences of my educational career.

Thank you to Dr. Leigh Sowerby for your supervision and guidance throughout this project. Your assistance in the shaping of this study and completing surgical interventions on cadaveric heads, as well as your expertise in the anatomy pertaining to my research, were all crucial to the success of this project.

Thank you to Dr. Katherine Willmore and Dr. Khadry Galil for their direction and supervision during the course of this project. Thank you for advising me through the writing process, helping me with statistical analyses, and keeping me on track to meet all my deadlines.

Thank you to Matthew Harris for pushing me in the right direction from the very beginning. You have provided me with ideas and suggestions that made this study possible. Thank you for your help during testing, scan analysis and statistical analyses. It has been a pleasure working with you.

Thank you to Dr. Thomas Jenkyn, Mark Neuert and Timothy Burkhart, from the Department of Mechanical and Materials Engineering, for allowing me to use your lab and testing equipment. Thank you for setting up the testing apparatus, teaching me how to use the

equipment and assisting me in performing the appropriate calculations. You have all been tremendously helpful throughout the course of this project.

Thank you to Donna Findlay, from the Diagnostic Imaging Centre at St. Joseph's Hospital, for being so generous and helpful during the CT scanning process. This project could not have been completed without you.

Thank you to Jacob Reeves and Nikolas Knowles, from the Department of Mechanical and Materials Engineering, for assisting with the use of the Mimics software and BMD measurements. Your help was greatly appreciated, without which this project would not have been complete.

Thank you to Daniel Tietelbaum and Niloofar Ahanchin, my wonderful volunteers. I am truly grateful for all your help. The smooth and efficient execution of this study would not have been possible without you.

Thank you to Haley Linklater and Kevin Walker in the Western Gross Anatomy Lab for their help with specimen acquisition, obtaining demographic information from the donors, preparing the morgue for specimen potting, as well as unpotting the specimens once I was finished. I would not have been able to complete my research without your assistance and guidance.

Thank you to the donors and their families for making such a selfless and positive contribution to research. I will forever be grateful for the gift your loved ones have provided. I am extremely fortunate to have had the opportunity to learn so much through your generosity.

Thank you to my Clinical Anatomy colleagues for making my time in this program so memorable. It has been a pleasure working with all of you and these past two years would not have been the same without your love and support.

Thank you to my wonderful family for your constant encouragement and support. You have consistently taught me the value of higher education and provided me with the guidance needed to acquire my goals. You have always been there for me and I would not be where I am now without you.

Table of Contents

Abstract	ii
Co-Authorship Statement.....	iii
Acknowledgments.....	iv
Table of Contents	vi
List of Tables	ix
List of Figures	x
List of Appendices	xii
List of Abbreviations	xiii
Chapter 1	1
1 Literature Review	1
1.1 Anatomy of the Orbit	1
1.2 Orbital Fractures	2
1.2.1 Etiology and Incidence	2
1.2.2 Mechanisms of Orbital Fractures.....	3
1.2.3 Complications	4
1.2.4 Restorative Surgery.....	5
1.3 Bone Mineral Density	6
1.4 Osteomeatal Complex and Uncinate Process	7
1.5 Paranasal Sinuses	9
1.6 Rhinosinusitis.....	10
1.7 Functional Endoscopic Sinus Surgery	11
1.7.1 Introduction.....	11
1.7.2 Uncinectomy.....	12
1.7.3 Maxillary Antrostomy.....	13

1.7.4	Ethmoidectomy	13
Chapter 2	15
2	Introduction	15
2.1	Purpose of Study	15
2.2	Study Objectives	16
2.3	Hypothesis.....	16
Chapter 3	17
3	Methods.....	17
3.1	Subject Data	17
3.2	Preliminary Study	18
3.3	Actual Study.....	18
3.3.1	Potting and FESS	19
3.3.2	Globe Injections	19
3.3.3	Testing.....	20
3.3.4	CT Scanning.....	21
3.3.5	Bone Mineral Density	21
3.3.6	Statistical Analysis.....	22
Chapter 4	24
4	Results	24
4.1	Preliminary Study	24
4.2	Actual Study.....	24
4.2.1	Fracture Pattern Distribution.....	24
4.2.2	Impact Energies	26
4.2.3	Bone Mineral Density	28
4.2.4	Summary of Results	29

Chapter 5.....	30
5 Discussion	30
5.1 Interpretation of Results.....	30
5.2 Anatomical Significance.....	30
5.3 Clinical Implications.....	34
5.4 Strengths and Limitations	34
5.5 Future Directions	35
5.6 Conclusion	36
Bibliography	38
Appendix A: Rights and Permissions	42
Appendix B: Permissions to Scholarship@Western.....	43
Curriculum Vitae	44

List of Tables

Table 1. Specimen Information (n=14).....	18
Table 2. Analysis of fracture pattern distribution of cadaveric heads following each round of impact during testing. Eight out of ten fresh-frozen cadaveric heads were tested to compare the fracture threshold on operated vs. non-operated control. Fractures of both the medial wall and orbital floor were seen after one round of impact (n=1), two rounds of impact (n=3), three rounds of impact (n=2), or not at all (n=2).	25
Table 3. Peak energies required to induce an orbital fracture on the surgical and non-surgical sides, with the associated fracture pattern, for each cadaveric head.....	27
Table 4. Average ρ_{APP} values, calculated using Materialise Mimics® and LabVIEW System Design Software, for each cadaveric head and associated fracture site via pre-surgical scans.	28

List of Figures

Figure 1. Schematic of the bones of the orbit	1
Figure 2. (A) Schematic representing the hydraulic theoretical mechanism of the orbital floor fracture. As the globe is repulsed by a force (large arrow), the intraorbital pressure is increased, force is transmitted to all walls of the orbit (small arrows), and the floor is fractured. (B) Schematic representing the buckling theoretical mechanism of the orbital floor fracture. Force (large arrow) is directed toward the inferior orbital rim and transmitted along the orbital floor, creating a fracture (small arrows).....	4
Figure 3. Schematic of the osteomeatal complex, located between the middle turbinate and lateral wall of the nasal cavity, where sinus drainage occurs.....	8
Figure 4. The uncinat process (U) running parallel to the lateral nasal wall, which holds the middle turbinate (M).....	9
Figure 5. Schematic of the paranasal sinuses (frontal, sphenoid, ethmoid, and maxillary)....	10
Figure 6. The uncinat process (U) has been backfractured to reveal the maxillary sinus ostium (Max). The middle turbinate (M) is seen on the lateral nasal wall.....	13
Figure 7. The ethmoid labyrinth (EL) can be visualized between the middle turbinate (M) and medial orbital wall. Ethmoid air cells have been surgically been removed.....	14
Figure 8. 4” PVC pipe filled with dental cement and cadaveric head fixed within for stability during testing.....	19
Figure 9. (A) Globe injection performed to restore ocular pressure. (B) Intraocular pressure measured with a Schiottz tonometer.....	20
Figure 10. (A) Testing apparatus consisting of a vertical plastic tube with 0.2 m increments to measure drop height. (B) Impact device with a metal nose to deliver the impact force.....	21

Figure 11. Pre-surgical CT scan of specimen 1869. Medial orbital wall on the surgical side (blue), and orbital floor on the non-surgical side (red) were isolated for BMD measurement.....22

Figure 12. (A) Pre-surgical CT scan of specimen 1869. (B) Medial orbital wall fracture (red) seen on the surgical side post-surgery. (C) Orbital floor fracture (blue) seen on the non-surgical side post-surgery, along with medial orbital wall fracture (red) on surgical side.....25

Figure 13. Analysis of fracture pattern distribution of cadaveric heads following testing. Heads (n=6) were impacted on both the surgical and non-surgical sides with all heads acquiring a medial wall fracture on the surgical side and an orbital floor fracture on the non-surgical side. Fisher’s exact test ($p < 0.01$).....26

Figure 14. Analysis of impact energies inducing post-surgery fractures. The peak impact energies required to induce orbital fractures were analyzed using GraphPad Prism 6 (surgical, n=6; non-surgical, n=6). The increase in energy required to induce a fracture on the non-surgical side was not significant (paired two tailed t-test; $p > 0.05$). Data are presented as mean \pm SD.....28

Figure 15. Changes in BMD among various impact energies. **A)** Changes in BMD among the impact energies for the medial orbital wall on the surgical side (unpaired two tailed t-test; $p > 0.05$). **B)** Changes in BMD among the impact energies for the orbital floor on the non-surgical side (one-way ANOVA; $p > 0.05$). Data were analyzed using GraphPad Prism 6 and are presented as mean \pm SD.....29

List of Appendices

Appendix A: Rights and Permissions.....	42
Appendix B: Permissions to Scholarship@Western.....	43

List of Abbreviations

ABRS – Acute bacterial rhinosinusitis

BMD – Bone mineral density

CRS – Chronic rhinosinusitis

CT – Computed tomography

DXA – Dual energy x-ray absorptiometry

FESS – Functional endoscopic sinus surgery

HU – Hounsfield units

INCS – Intranasal corticosteroids

OMC – Osteomeatal complex

QCT – Quantitative computed tomography

SD – Standard deviation

TIVA – Total intravenous anesthesia

ρ_{APP} – Apparent density

Chapter 1

1 Literature Review

1.1 Anatomy of the Orbit

The orbit is a bony pyramidal shaped region bounded by a roof, floor, and medial and lateral walls (Figure 1). The total volume of the bony orbit is approximately 30 mL, of which the globe occupies 7 mL. The orbit is an intimate and complex relation between seven bones: frontal, sphenoid, ethmoid, zygomatic, lacrimal, palatine, and maxilla (Gart & Gosain, 2014). The roof of the orbit is formed by the frontal and sphenoid bones. It separates the orbital contents from the anterior cranial fossa. The medial wall of the orbit is formed by the maxilla, lacrimal, orbital plate (lamina papyracea) of the ethmoid, and the palatine bones. The medial orbital wall is the thinnest wall of the orbit, along with the orbital floor. The ethmoid bone lies posterior to the lacrimal bone and separates the medial wall of the orbit from the upper part of the nasal cavity. It is profusely pneumatized by ethmoid air cells, making the medial wall fragile, hence the term *lamina papyracea* (paper thin) (Braffman, Naidich, & Chaneles, 1997; Morris, Liliav, & Cohen, 2014). The floor is comprised of the maxillary, zygomatic, and palatine bones. The lateral wall of the orbit is formed by the zygomatic bone and the greater wing of the sphenoid. It is the thickest and strongest wall of the orbit (Braffman et al., 1997).

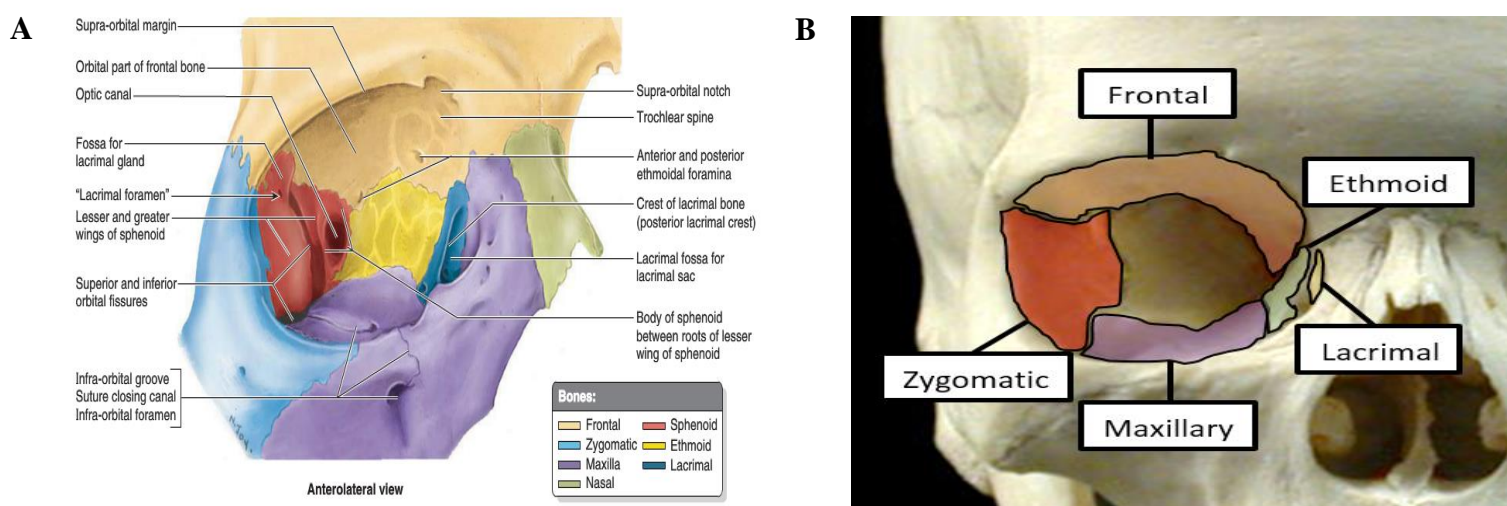


Figure 1. Schematic of the bones of the orbit.*

A) *Reprinted from Moore's Clinically Oriented Anatomy 7th Ed, by Moore, K.L., Dalley, A.F., & Agur A.M.R. (2013), with permission from Lippincott, Williams & Wilkins

B) *Reprinted and modified with permission from Galil (2004), <http://www.drgalil.ca/skull/index.htm>

1.2 Orbital Fractures

1.2.1 Etiology and Incidence

Orbital fractures are among the most common mid-facial fractures (Brown, Ky, & Lisman, 1999). Epidemiological trends with respect to the etiology of specific orbital injuries change from time to time, depending on the population being studied, its demographics and social behaviours (Hwang, You, & Sohn, 2009). Hwang *et al.* (2009) conducted a study to evaluate the natural history of orbital bone fractures in 391 cases over a 12 year period. The highest frequency of orbital bone fractures occurred in the 21 to 30 year (32.5%) age group with fractures occurring predominantly in males. The most common causes of orbital bone fractures included assault or nonviolent traumatic injury (57.5%), vehicle accidents (15.6%), sports injuries (10.7%), falls (8.7%), work-related injuries (5.9%), and others (1.5%). Similar results were found in a study analyzing the prevalence of zygomatico-orbital fractures in 2,067 patients over a 10 year period. In this study, the major cause of these fractures was found to be assault (46.6%), followed by falls (22.6%) and motor vehicle accidents (13.3%). Fractures occurred predominantly in males (80.2%) and the peak incidence was in the 20-30 year range (Ellis, El-Attar, & Moos, 1985). Therefore, orbital fractures are frequent occurrences in the younger adult male population and causality is related to violent or nonviolent trauma rather than disease or surgery.

The orbit tends to be particularly susceptible to fractures due to its exposed position and thin bones. External impact to this region may cause blowout fractures, which may be accompanied by defects of the orbital floor (Gosau *et al.*, 2011). Orbital floor defects range from 27 to 250 mm² and may be identified as any abnormality in the orbital floor, such as a fracture, a hole, or simply a displaced piece of bone (Birkenfeld *et al.*, 2012). The term ‘blowout’ fracture is used to refer to a syndrome in which the orbital wall is fractured, usually at its weakest points, and is normally due to a force impacting on the orbital soft tissue (Ahmad *et al.*, 2003; Burm *et al.*, 1999). A ‘pure’ blowout fracture is one in which a fracture of the orbital wall occurs without the involvement of the orbital rim. If the orbital rim is fractured in conjunction with the orbital wall, the term ‘impure’ fracture is used (Ahmad *et al.*, 2003; Brown *et al.*, 1999; Gart & Gosain, 2014). Pure orbital floor fractures can be found in 22 to 47 percent of orbital injuries, and represent up to 45 percent of all pediatric facial fractures (Gart & Gosain, 2014). The orbital

floor has a size of approximately 30 x 20 mm (width x length, respectively), and the weight of the orbital tissue is about 35 g (Birkenfeld et al., 2012). Though the orbital floor is most commonly involved in a blowout fracture, the associated injury may impact the medial orbital wall as well (Ahmad et al., 2003). In fact, the medial orbital wall damage is seen frequently in association with a fracture of the orbital floor (Yeo & Kim, 2015). However, despite its thin nature, the medial orbital wall is less likely to fracture than the orbital floor. Jank *et al.* (2003) gathered data from 424 patients with orbital fractures, over a six-year period. Isolated medial orbital wall fractures in these patients were found to be quite rare (0.2%), compared to those of the floor (84.2%). Hwang *et al.* (2009) also found orbital floor fractures to be the most common (26.9%), followed by medial orbital wall fractures (13.3%), with a male predominance among all injuries and ages. Similarly, Brown *et al.* (1999) performed a retrospective review of 250 charts of patients with orbital fractures and found the most common type of fracture to be that of the orbital floor (58%). Eighty-five of the 250 patients had isolated fractures and the most common type was a pure orbital fracture (65%), followed by a medial wall fracture (22%). Pure orbital fractures are twice as common as impure ones, and the medial wall is fractured concomitantly in approximately 30% of floor fractures.

1.2.2 Mechanisms of Orbital Fractures

Orbital blowout fractures were first described by Lang in 1889. Several mechanisms behind orbital fractures have been presented (Gart & Gosain, 2014). In 1901, René Le Fort concluded that blowout fractures occurred as a result of direct trauma to the rigid inferior orbital rim, transmitting the force posteriorly and causing a compression fracture of the orbital floor. This is known as the “buckling theory” (Figure 2B). In 1948, this contention was challenged by Raymond Pfeiffer who proposed the “hydraulic theory” (Figure 2A), which states that repulsion of the globe elevates intraorbital pressure, resulting in direct compression of the orbital floor and fracturing of the thin bone (Brown et al., 1999; Rhee et al., 2002; Warwar, Bullock, Ballal, & Ballal, 2000).

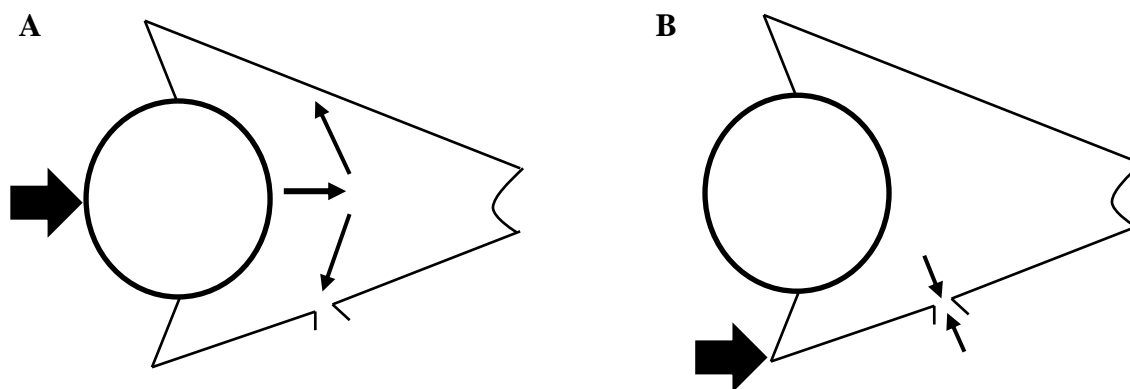


Figure 2. (A) Schematic representing the hydraulic theoretical mechanism of the orbital floor fracture. As the globe is repulsed by a force (large arrow), the intraorbital pressure is increased, force is transmitted to all walls of the orbit (small arrows), and the floor is fractured. (B) Schematic representing the buckling theoretical mechanism of the orbital floor fracture. Force (large arrow) is directed toward the inferior orbital rim and transmitted along the orbital floor, creating a fracture (small arrows).

More recently, a third theory was formulated by Erling *et al.* (1999), known as the “globe-to-wall” theory. This theory is an extension of Pfeiffer’s original theory and states that a direct “globe-to-wall” impact is responsible for some orbital blowout fractures. If the globe is displaced to within 2.5 cm of the orbital apex, the globe itself will fracture the orbital wall. This fracture mechanism is less recognized as a cause of orbital fractures (Brown *et al.*, 1999).

1.2.3 Complications

Common complications of orbital fractures include diplopia, enophthalmos/exophthalmos and abnormalities of the infraorbital nerve (Birkenfeld *et al.*, 2012). Diplopia, also known as double vision, is the most common complication of orbital floor defects (Gosau *et al.*, 2011). This is supported by the study performed by Hwang *et al.* on 391 orbital bone fracture patients. Upon physical examination of these patients before surgery, diplopia was found to be the most common associated complication (61.6%), followed by infraorbital hypoesthesia (51.4%), enophthalmos (46.3%), and limitation of ocular movement.

Jank *et al.* (2003) found that orbital fractures with the involvement of the medial orbital wall showed a significantly higher incidence of diplopia and exophthalmos than fractures without the involvement of the medial orbital wall. Emphysema is a common benign complication of fractures associated with the medial orbital wall. Other rare cases include optic neuropathy and pneumomediastinum (Cruz & Eichenberger, 2004).

Incidences of ocular injuries have also been reported in several cases associated with orbital bone fractures. These include ruptured globe, vitreous hemorrhage, corneal abrasion, afferent pupillary defect, retinal detachment, dislocated lens, choroidal rupture, and retinal edema. While reviewing the charts of 250 patients with orbital fractures, Brown *et al.* (1999) found the incidence rate of ocular injury to be 17.1%. Other common injuries associated with orbital bone fractures include head and neck injuries. These involve brain injuries with cranial blood vessel disruption, altered levels of consciousness, cervical spine injuries, and optic nerve injuries (Hwang *et al.*, 2009).

1.2.4 Restorative Surgery

Immediate surgical intervention to restore the anatomic structure of the orbit is required to improve orbital appearance and visual function (Gosau *et al.*, 2011). Delayed surgery is not preferable due to tissue scarring, potential contractures around fracture sites, increased hemorrhage risk, and difficulty in isolating the infraorbital nerve (Hwang *et al.*, 2009). Most studies define immediate repair as occurring within 24 to 48 hours (Gart & Gosain, 2014). Common indications for surgery include diplopia, enophthalmos, and infraorbital hypoesthesia (Birkenfeld *et al.*, 2012; Cruz & Eichenberger, 2004; Hwang *et al.*, 2009).

The primary objective of surgically reconstructing the orbital floor is to release and reposition entrapped soft tissue contents, and reestablish the normal orbital volume (Cruz & Eichenberger, 2004; Gosau *et al.*, 2011). Surgical techniques vary as a result of differences in management by surgical specialists, their background, their choices regarding the approach, materials used to perform the reconstruction, timing of surgical intervention, as well as personal experiences (Cruz & Eichenberger, 2004; Yeo & Kim, 2015). The transconjunctival approach is strongly favored over the subciliary approach, as it allows quick access to the surgical field and reduces the risk of lower eyelid retraction (Cruz & Eichenberger, 2004; Gosau *et al.*, 2011). In the transconjunctival (internal) approach, the inner conjunctiva is incised below the tarsal level, from the caruncle medially to the lateral fornix. The septal plane is then followed until the orbital rim. In contrast, the subciliary (external) approach consists of a skin incision made 1-2 mm below and parallel to the lower margin of the eyelid. A skin-muscle flap dissection is carried down to the tarsal plate, followed by the preseptal plane. A periosteal incision is then performed to expose the infraorbital rim. Once necessary, alloplastic implants are used to repair the orbital floor (Pausch, Sirintawat, Wagner, Halama, & Dhanuthai, 2015). Polydioxanone is a widely used reconstruction material

for repairing most small to medium orbital floor defects. For larger fractures, the use of titanium mesh is recommended (Birkenfeld et al., 2012; Gosau et al., 2011).

In the case of a medial orbital wall fracture, Lynch incisions have been known to provide good exposure. A curvilinear incision is made just below the medial end of the eyebrow and curved to the medial canthus to access the frontal process of maxilla, as well as the lamina papyracea. However, the Lynch incision leaves a noticeable scar and tends to be invasive (Cruz & Eichenberger, 2004). Recently, multiple groups have recommended the use of the transcaruncular approach as it allows for safe exposure and direct visualization of the medial wall, while inhibiting the formation of cutaneous scars (Morris et al., 2014). The conjunctiva near the caruncle is incised and the dissection performed medially to the posterior lacrimal crest. The periosteum just beneath this crest is incised and the periorbital elevated to access the medial orbital wall (Oh et al., 2003). For combined orbital floor and medial wall fractures, an extension of the transconjunctival approach for the floor into a transcaruncular approach for the medial wall has shown to be useful (Morris et al., 2014).

1.3 Bone Mineral Density

Bone mineral density (BMD) is a major factor affecting fracture risk. Numerous other factors apart from BMD regulate fracture risk as well, however BMD is probably the most important one (Hamdy, 2016).

The most common method for measuring BMD is called Dual Energy X-Ray Absorptiometry (DXA). It uses X-rays at two energy levels and works on the principle that, as X-rays pass through body tissues, they are attenuated to a different extent in different tissue types. It is a safe and painless procedure, with a very small amount of radiation exposure (Winzenberg, 2011).

In the decade before DXA scanners came to light, computed tomography (CT) was introduced. Initially for head scanning, CT scanners later became available for the whole body as well. Soon after, the quantitative capability of CT (QCT) was applied to the skeleton (Adams, 2009). Quantitative computed allows tissue density to be extrapolated from attenuation data captured in a CT scan (Reeves et al., 2016).

Computed tomography utilizes X-rays and provides images based on the linear X-ray absorption coefficients of the tissues through which it passes. All clinical body CT scanners are similarly calibrated to the X-ray attenuation of water, resulting in CT numbers which are measured in Hounsfield Units (HU), in relation to water being 0 HU. Areas, such as bone, absorb more X-rays and have a high HU number (Adams, 2009). Unfortunately, not all clinical CT scans are calibrated properly using a density phantom. To use uncalibrated scans, post-hoc calibration methods are required (Reeves et al., 2016). For the purposes of this study, a multivariate regression model was used to develop a density calibration.

1.4 Osteomeatal Complex and Uncinate Process

The osteomeatal complex (OMC), shown in Figure 3, is a small region located between the middle turbinate of the nasal cavity and the lateral nasal wall, in the middle meatus. The OMC is a site of drainage for various paranasal sinuses. An abnormality in any one of the components of the OMC can lead to improper drainage of these sinuses, thereby increasing the risk for chronic rhinosinusitis. The uncinate process and ethmoid bulla are two main structures encountered within the OMC (Srivastava & Tyagi, 2015).

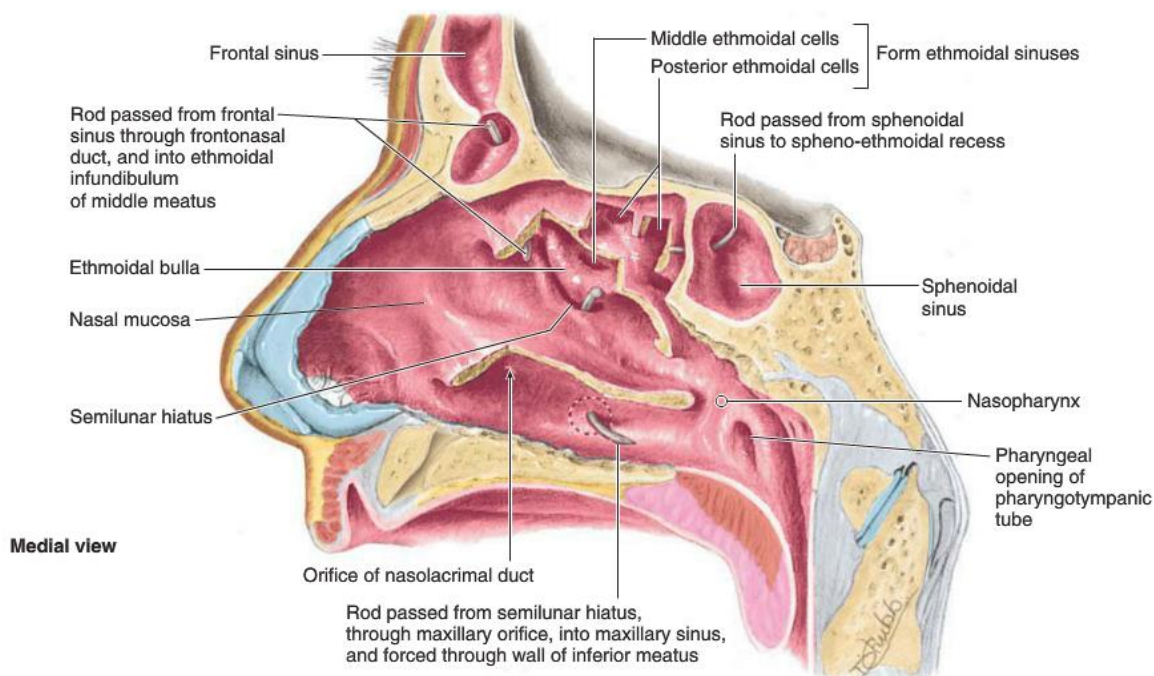


Figure 3. Schematic of the osteomeatal complex, located between the middle turbinate and lateral wall of the nasal cavity, where sinus drainage occurs.*

*Reprinted from Moore's Clinically Oriented Anatomy 7th Ed, by Moore, K.L., Dalley, A.F., & Agur A.M.R. (2013), with permission from Lippincott, Williams & Wilkins

The uncinete process (Figure 4) is an L-shaped, bony leaflet which runs from an anterosuperior to posteroinferior direction, parallel to the anterior surface of the ethmoid bulla on the lateral nasal wall. It forms the anterior border of the hiatus semilunaris (infundibulum). The infundibulum is the location of the OMC. Posteroinferiorly, the uncinete process attaches to the inferior turbinate. The ascending anterior margin of the process may either be attached to the lamina papyracea (up to 52%), and/or to the skull base or the middle turbinate (Lund et al., 2014; Srivastava & Tyagi, 2015; Tuli, Sengupta, Munjal, Kesari, & Chakraborty, 2013). The significance of this variation has to do with altered frontal sinus drainage. When the uncinete process is attached to the lamina papyracea, the frontal sinus drains into the middle meatus, medial to the uncinete process attachment. When attached to the skull base or middle turbinate, the uncinete process changes the pattern of frontal sinus drainage into the infundibulum, which is now located lateral to the uncinete process attachment. This change may be a determining factor in the development of frontal sinusitis (Gnanavelraja et al., 2014).

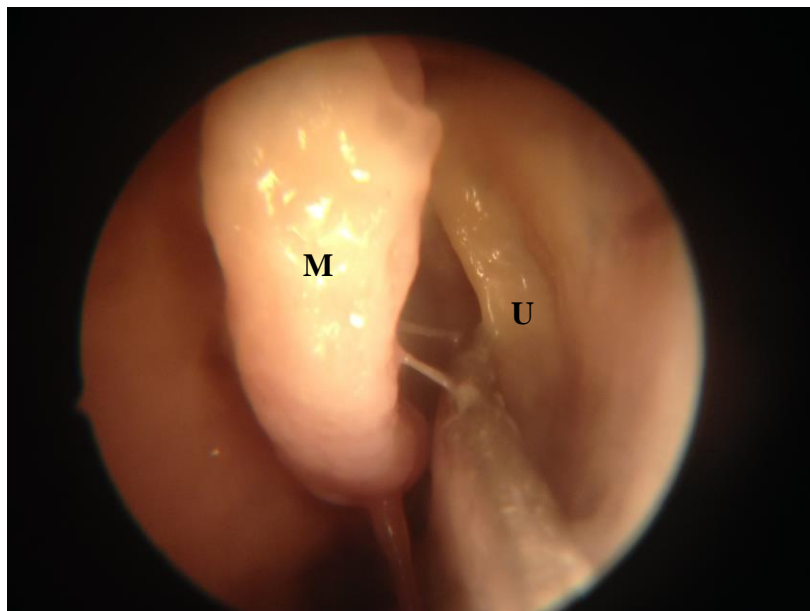


Figure 4. The uncinete process (U) running parallel to the lateral nasal wall, which holds the middle turbinate (M).

1.5 Paranasal Sinuses

The paranasal sinuses are air-filled bony cavities within the skull, acting as extensions of the respiratory portion of the nasal cavities. They consist of paired maxillary, sphenoid, ethmoid, and frontal sinuses, named according to the skull bone in which they reside (Figure 5). The ethmoid sinuses consist of anterior and posterior ethmoid air cells. Through narrow ostia, all four sinuses connect to the superior (posterior ethmoid cells and sphenoid sinus) and middle (anterior ethmoid cells, frontal and maxillary sinuses) meati of the nasal cavity (Figure 3) (Lund et al., 2014).

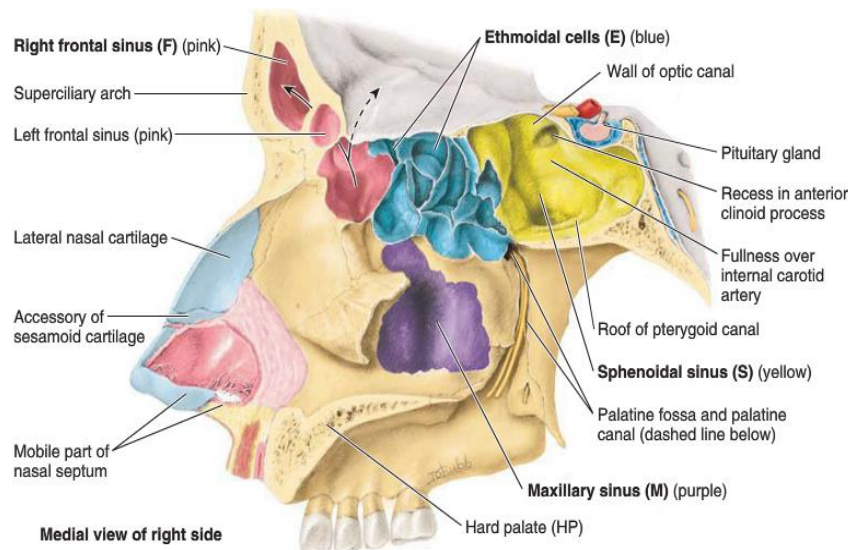


Figure 5. Schematic of the paranasal sinuses (frontal, sphenoid, ethmoid, and maxillary).*

*Reprinted from Moore's Clinically Oriented Anatomy 7th Ed, by Moore, K.L., Dalley, A.F., & Agur A.M.R. (2013), with permission from Lippincott, Williams & Wilkins

Normal functions of the paranasal sinuses include decreasing the weight of the skull, increasing resonance of voice, buffering against blows to the face, and providing a surface area for warming and humidifying inspired air. These sinuses may become blocked with inflammation or swelling in the nasal epithelium. The normal circulation of mucus within the sinuses is disrupted, leading to the occurrence of rhinosinusitis (Pullen, 2010).

1.6 Rhinosinusitis

Rhinosinusitis is an inflammatory disease of the sinuses. It is a very common condition, affecting approximately 1 in 8 adults (Kaplan, 2013). This condition may be acute, lasting up to four weeks, or present with chronic symptoms lasting more than twelve weeks. It involves inflammation in at least one of the paranasal sinuses. Inflammation affects not only the sinuses, but also the mucosa of the nose, hence the move towards the term 'rhinosinusitis' rather than 'sinusitis'. Common symptoms include nasal congestion, pain or pressure in the region of the sinuses affected, nasal obstruction, nasal discharge, and decreased sense of smell (Kaplan, 2014).

Acute bacterial rhinosinusitis (ABRS) is an inflammatory disease of bacterial infection that initiates an inflammatory response in the nasal mucosa and sinuses. This leads to constriction of nasal passages and poor mucus drainage from the sinuses. Treatment, such as antibiotics, are recommended for at least 10 to 14 days for ABRS. Intranasal corticosteroids (INCS) can also be used during conditions of mild to moderate ABRS to reduce inflammation, promote sinus

drainage, and improve sinus ventilation. Significant benefit has been shown to be associated with 15 to 21 days of INCS therapy added to antibiotic therapy in patients with ABRS (Kaplan, 2014).

Chronic rhinosinusitis (CRS) has a reported prevalence of 5% in Canada (Kaplan, 2013). A rising prevalence of CRS has been reported since 1991 (Damm, Quante, Jungehuelsing, & Stennert, 2002). The prevalence increases with age, is higher for women, and individuals with a history of allergies. A wide range of inflammatory patterns may act together with mucociliary and/or structural abnormalities to give rise to the development of CRS. The multifactorial etiology of CRS also includes genetic factors, environmental influences, occupational factors, infection, allergy, immune dysfunction, as well as systemic diseases (Orlandi et al., 2016). Although CRS is distinct from ABRS, antibiotic prescriptions are comparable for both types of disease. In the case of CRS, if medical therapy fails, sinus surgery is often required to restore ventilation, relieve obstruction, and optimize topical medication delivery (Kaplan, 2013).

1.7 Functional Endoscopic Sinus Surgery

1.7.1 Introduction

The technique of functional endoscopic sinus surgery (FESS) was introduced in the United States, in 1985, by Kennedy *et al.* (Bublik, Herman, & Younis, 2009). FESS is a minimally invasive, safe, and effective procedure, routinely performed by otolaryngologists for the management of sinonasal pathology. This surgery is performed more frequently in adults than in children. Most sinus disease in children is limited to the OMC and adenoids. The theory behind FESS is to re-establish drainage from the maxillary, ethmoid, sphenoid, and frontal sinuses and optimize topical medication delivery (Bublik et al., 2009). Senior *et al.* (1998) reported that symptoms improved in 66 of 72 (91.6%) patients following endoscopic sinus surgery, with a mean follow-up time of 7.8 years. Damm *et al.* (2002) analyzed 279 patients with a history of sinus surgery and reported an improvement in quality of life for 85% of their patient population, with a mean follow-up time of 31.7 months. Responsible for this improvement were a decrease of nasal obstruction (84%), headache (82%), and postnasal drip (78%).

Complications of FESS tend to be divided into ‘minor’ and ‘major’ categories. Minor complications may include bleeding, infection, ostial stenosis, tooth or lip numbness, and recurrence of disease (McMains, 2008). Major complications of FESS that have been reported

include cerebrospinal fluid leak, meningitis, hemorrhage, and orbital injuries (Krings et al., 2014; McMains, 2008). In a study examining the frequency of major complications following both primary and revision FESS in a cohort of nearly 80,000 patients, it was reported that the risk of such complications was low at 0.36% and 0.46%, respectively. (Krings et al., 2014).

Surgery is typically performed under general anesthesia, and total intravenous anesthesia (TIVA). TIVA has been shown to minimize blood loss (Wormald et al., 2005). Neurosurgical patties with a topical decongestant are placed into the nasal cavity and middle meatus, if accessible. Before beginning any dissection, the neurosurgical patties are removed and 1% lidocaine with 1:100,000 epinephrine is injected into the bilateral sphenopalatine areas, middle turbinate, inferior turbinate, uncinate process, and septum (Bublik et al., 2009). There are various different procedures involved with FESS; however, for the purposes of this study, an uncinectomy was performed with a concurrent maxillary antrostomy and anterior/posterior ethmoidectomy.

1.7.2 Uncinectomy

Uncinectomy is the first step performed in FESS (Singhania, Bansal, Chauhan, & Soni, 2012). A complete uncinectomy is necessary in order to perform a complete maxillary antrostomy and prevent mucus recirculation. Singhania *et al.* (2012) recommend the swing door technique as it allows for removal of the uncinate process in order to fully visualize the maxillary ostium, without penetrating the lamina papyracea. Backbiting forceps are used to identify the uncinate process, hiatus semilunaris, and infundibulum by placing the instrument underneath the uncinate process and reflecting it anteriorly. As shown in Figure 6, the uncinate process is backfractured to reveal the medial orbital wall and maxillary sinus ostium (Bublik et al., 2009). A 90-degree blakesley forceps is then used to remove the uncinate along the anterior axillary line.

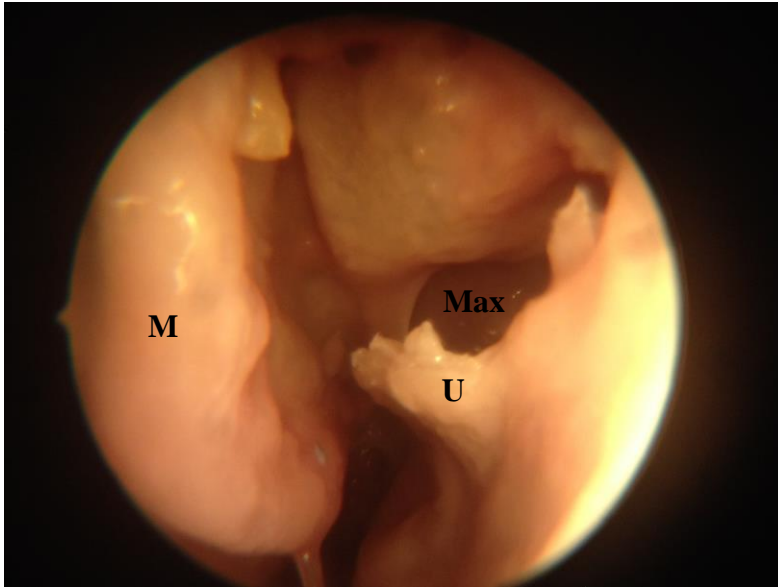


Figure 6. The uncinate process (U) has been backfractured to reveal the maxillary sinus ostium (Max). The middle turbinate (M) is seen on the lateral nasal wall.

1.7.3 Maxillary Antrostomy

The superior border of the ostium of the maxillary sinus demarcates the junction between the medial orbital floor and lamina papyracea. A maxillary antrostomy is performed using through-cutting instrumentation to identify the medial orbital floor and dissection is carried towards the posterior wall of the maxillary sinus to enlarge the ostia. The basal lamella of the middle turbinate delineates the anterior from posterior ethmoid cells (Bublik et al., 2009).

1.7.4 Ethmoidectomy

The ethmoid labyrinth (Figure 7) is located between the middle turbinate and the medial orbital wall. The width of the ethmoid increases from anterior to posterior because of the conical structure of the orbit. An anterior ethmoidectomy begins with the identification of the second lamella of the ethmoid bulla (the first lamella being the uncinate process). After opening the ethmoid bulla, the anterior ethmoid cells can be visualized for surgical removal (Bublik et al., 2009).

To continue with a posterior ethmoidectomy, the third lamella (basal lamella of the middle turbinate) is identified as it is the anatomical separation between the anterior posterior ethmoid cells. This area is entered with suction, and through-cutting instrumentation and a microdebrider

are used to remove septations. This dissection is performed in a posterior to anterior direction (Bublik et al., 2009).

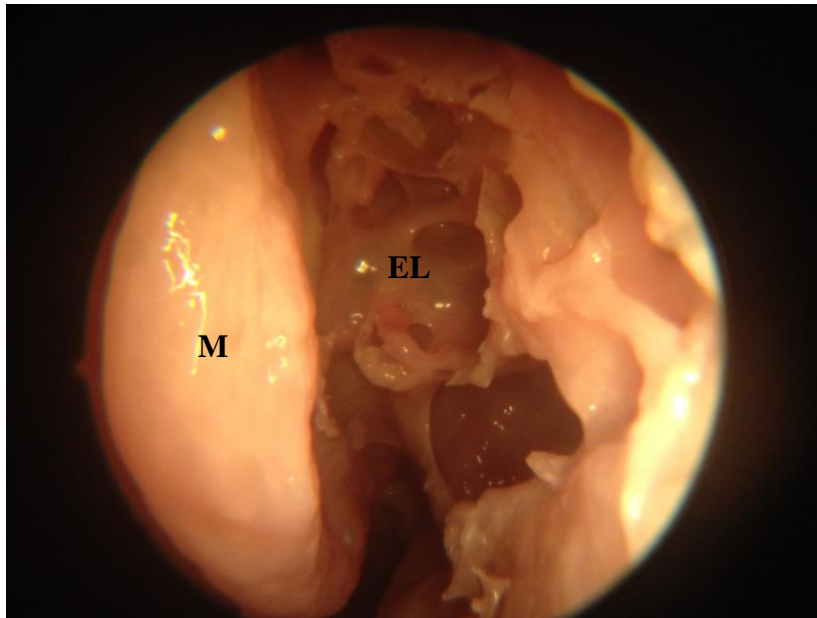


Figure 7. The ethmoid labyrinth (EL) can be visualized between the middle turbinate (M) and medial orbital wall. Ethmoid air cells have been surgically removed.

Chapter 2

2 Introduction

2.1 Purpose of Study

Currently, no literature exists to establish the effect of sinus surgery on orbital fracture risk in patients. Kellman and Schmidt (2009) performed a similar study in which the paranasal sinuses were obliterated and orbital fractures were induced. Their conclusion was that, without the sinuses, there is an increased risk of globe rupture. They hypothesized that the paranasal sinuses function as crumple zones for trauma to the orbital area. Our question is similar: to assess whether there is a greater risk of orbital fracture (as opposed to globe rupture) in post-sinus surgery patients.

Previous studies have shown that the hydraulic theory induces trauma to the globe that is dispersed throughout the orbit, resulting in orbital floor fractures and, in some cases, the medial wall as well depending on the amount of energy transmitted (Kellman & Schmidt, 2009). This further supports the use of this mechanism for the purposes of our study. Recent published literature regarding orbital fracture forces and mechanisms has also detailed the force required to induce orbital fractures. Rhee *et al.* (2002) utilized an increasing trauma force in fresh human cadavers to induce orbital floor fractures at an energy of 2.9 J (drop height of 30 cm) or above, with medial wall fractures seen with energies of 4.9 J (drop height of 50 cm) or above. This suggests that the most common location of fractures is the orbital floor. These findings are consistent with previous studies which have reported floor fractures caused by energies ranging from 2.08 to 3.28 J (Green *et al.*, 1990).

What is not understood is how FESS (in this study an uncinectomy, maxillary antrostomy, and ethmoidectomy) affects the skeletal strength of the bony orbit. Resection of the uncinete process and ethmoid air cell septations, as well as skeletonization of the lamina papyracea, may predispose a patient to post-surgical fractures. As mentioned previously, the medial orbital wall is less likely to fracture than the orbital floor. This may be due to the uncinete process of the ethmoid bone, as well as the bony septations of the ethmoid air cells, acting as buttresses for the medial orbital wall. This study aims to assess whether, following the intervention of sinus

surgery, there is a greater risk of medial orbital wall fracture vs. orbital floor blowout fracture (i.e. change in fracture pattern).

2.2 Study Objectives

The objectives of this study are to:

1. Evaluate the occurrence and pattern of post-FESS orbital fractures using computed tomography.
2. Compare the energy required to induce a fracture in the medial orbital wall versus the orbital floor, for both surgical and non-surgical orbits.

2.3 Hypothesis

It is hypothesized that FESS will change the fracture pattern by increasing the frequency of medial wall fractures seen in a cadaveric model, as well as reduce the energy required to induce a fracture in the medial orbital wall, compared to the orbital floor.

Chapter 3

3 Methods

3.1 Subject Data

For the purposes of this study, 4 fixed and 10 fresh cadaveric human heads were harvested from specimens in the Human Anatomy Lab at the University of Western Ontario. All data was obtained in accordance with the Anatomy Act of Ontario and Western's Committee for Cadaveric use in research, ethics approval #06232015. Fresh-frozen heads were removed from fresh, non-perfused cadaveric specimens and subsequently frozen in the morgue until they required thawing to perform necessary surgeries and testing procedures. Twenty-four hours before each procedure, the heads were defrosted by room temperature. Mean age was 79.5 ± 17.1 (age range 41-98) years with the study population consisting of 6 (43%) males and 8 (57%) females. Cause of death varied among donors. A detailed list containing all subject data is included in Table 1.

Table 1. Specimen Information (n=14).

	Specimen ID	Age	Sex	Cause of Death
Fixed (n=4)	1744	88	Female	NSTEMI, CAD, Diabetes, CHF
	1757	94	Female	Pneumonia, CHF Exacerbation
	1775	65	Male	Multiple Myeloma, Chronic Myelomonocytic Leukemia, Type 2 Diabetes, Anemia
	1855	96	Female	Diabetes
Fresh-frozen (n=10)	1864	41	Female	Metastatic GI Neuroendocrine Tumor, Renal Failure, Hyperkalemia, GI
	1869	88	Male	Cardiorespiratory Arrest, Large MCA stroke
	1883	88	Male	Adenocarcinoma of Prostate with Metastases
	1894	84	Female	Dementia, Pneumonia, New onset atrial fibrillation
	1895	54	Female	Metastatic Breast Cancer
	1904	98	Male	Pneumonia, ASHD, Hyperthyroidism
	1906	81	Female	Dementia, Carcinoma of Lung
	1908	81	Male	Laryngeal Cancer, Advanced Shape of Cancer, Arrhythmia, COPD
	1945	91	Female	End Stage CHF
	1948	64	Male	AML, Cardiomyopathy

3.2 Preliminary Study

Using fixed (n=4) cadaveric heads, a preliminary study was conducted to test the protocol and narrow the range of energy required to produce orbital fractures. The protocol for this study is outlined below. FESS and globe injections were not performed on these heads.

3.3 Actual Study

The following methodology was performed on both fixed (n=4) and fresh-frozen (n=8) heads within this study, with the exception of FESS and globe injections which were performed solely on the fresh-frozen specimens.

3.3.1 Potting and FESS

Each head was potted in a 4" PVC pipe (obtained from Rona, Inc.), filled with dental cement (Denstone Golden, Modern Materials), for stability during testing (Figure 8). FESS was performed by a fellowship-trained board-certified rhinologist on one side of the head for each fresh-frozen specimen, while the other side served as control. The control and surgical side designations was by random selection. Pre- and post-operative CT scans were performed on all fresh-frozen heads for fracture identification.



Figure 8. 4" PVC pipe filled with dental cement and cadaveric head fixed within for stability during testing.

3.3.2 Globe Injections

Cadaver eyes tend to become flaccid with no measurable intraocular pressure. Globe injections were performed on all fresh-frozen heads for reinflation and restoration of intraocular tension to the normal value of 15 mmHg (Figure 9A). Between 2.5 and 4 mL of sodium chondroitin sulfate (40 mg/mL - sodium hyaluronate (16.5 mg/mL) solution (DisCoVisc, Ophthalmic Viscosurgical Device) was injected into each globe using a 27 gauge syringe. Intraocular pressure was confirmed through measurement with a Schiottz tonometer (Sklar Surgical Instruments; Figure 9B).

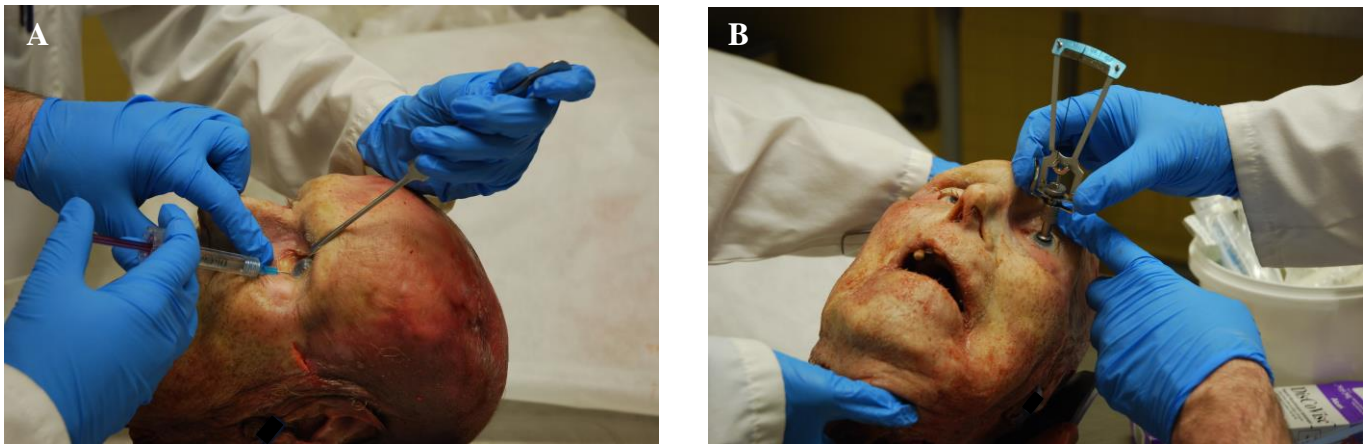


Figure 9. (A) Globe injection performed to restore ocular pressure. (B) Intraocular pressure measured with a Schiotz tonometer.

3.3.3 Testing

An impact device was constructed consisting of a vertical plastic tube (Figure 10A), with markings found at 0.2 m increments to measure drop height. A weight of 1.356 kg was used to deliver the impact force and a metal ‘nose’ was attached to the bottom of the weight to provide an impact area of 767 mm² (Figure 10B). The weight was fitted with an eye loop and a threaded cord allowed elevation of the weight within the tube. Positioning the nose over the orbit allowed accurate targeting of the weight to the impact point, which was the globe for this study.

Energy testing was commenced with the impact device at a drop height of 0.46 m for each fresh-frozen specimen. Energy delivered by the impact device was calculated using the following equation: $U = mgh$, where U = energy (Joules), m = mass of the impactor (kilograms), g = gravitational acceleration (meters per seconds squared), and h = height (meters). Drop heights ranged from 0.46 m to 0.56 m. Selection of the first side for impact (control side or surgical side) was randomized for each head. The impact energy level on one orbit, for each head, was repeated on the other orbit for that same head. After delivering one strike to the globe of each eye, the apparatus was removed and the heads underwent CT scanning. The procedure was repeated by dropping the weight from progressively higher heights until fractures were detected.



Figure 10. (A) Testing apparatus consisting of a vertical plastic tube with 0.2 m increments to measure drop height. (B) Impact device with a metal nose to deliver the impact force.

3.3.4 CT Scanning

All heads were scanned prior to surgery and after each round of energy testing. High resolution CT scanning, via a GE 750 HD scanner, was used to detect the presence of fractures. Axial scans were performed with a full tube rotation time of one second, and dose performance of 80 kV, on a bone algorithm. Each rotation captured 32 images with a slice thickness of 0.625 mm for each image and a detector coverage of 20 mm. CT scans were obtained from St. Joseph's Hospital, London, Ontario, Canada. All fractures were assessed and confirmed by a surgical resident in the Department of Otolaryngology, St. Joseph's Hospital.

3.3.5 Bone Mineral Density

Through the use of Materialise Mimics® (Mimics 16.0 for X64 Platform V 16.0.0.235), a software designed for medical image processing, the average apparent BMD values for each cadaveric head were extracted in the form of HU. These units were calculated for both the medial orbital wall on the surgical side, and the orbital floor on the non-surgical side, for each specimen by isolating these bony regions using pre-surgical CT scans (Figure 11).

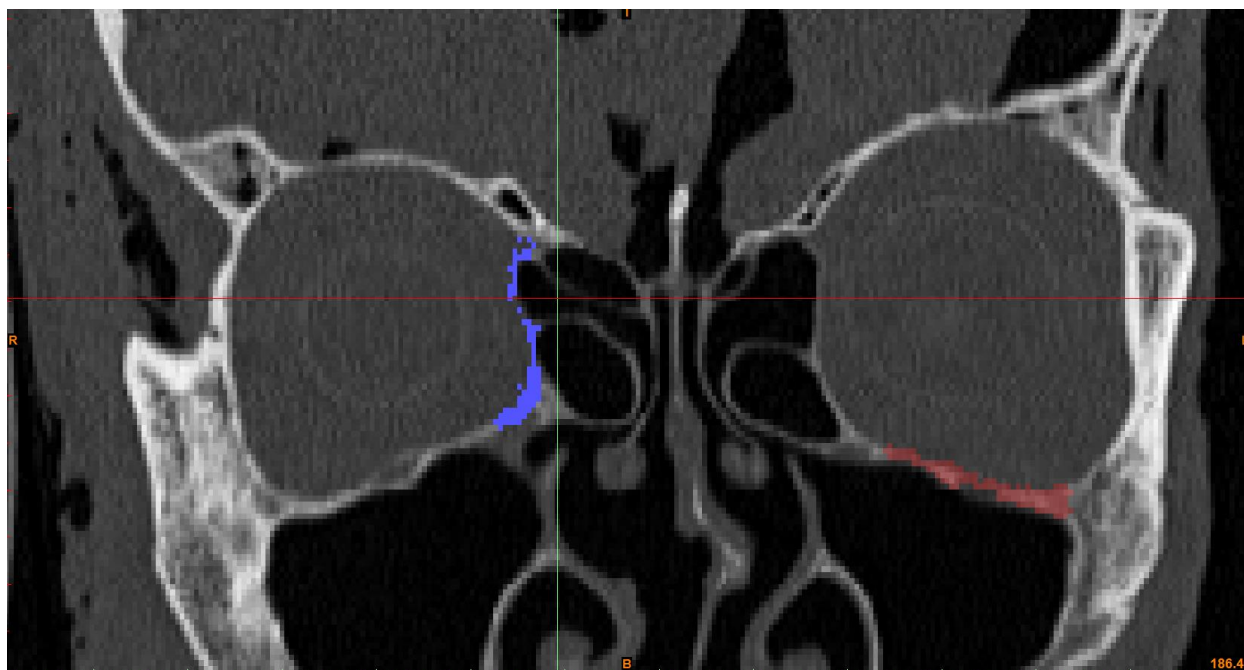


Figure 11. Pre-surgical CT scan of specimen 1869. Medial orbital wall on the surgical side (blue), and orbital floor on the non-surgical side (red) were isolated for BMD measurement.

HU were converted to average apparent density (ρ_{APP}) units using a custom code, written in the LabVIEW System Design Software, by an MSc candidate in the Faculty of Engineering at the University of Western Ontario. CT scans were calibrated with a SB3-H2O phantom, which uses a cortical bone surrogate and distilled water, to form a linear relationship between HU and ρ_{APP} . The average ρ_{APP} was estimated using a regression equation for the SB3-H2O phantom in units of grams/cubic centimeter (g/cm^3).

3.3.6 Statistical Analysis

All analyses were completed using GraphPad Prism 6 software. A Fisher's exact test was performed to analyze the difference in fracture pattern across heads. A paired two tailed t-test was performed to analyze the difference in impact energies between the medial orbital wall and orbital floor ($n=6$). An unpaired two tailed t-test was performed to analyze the changes in BMD among the various peak impact energies of the medial orbital wall ($n=6$). A one-way ANOVA was performed to analyze the changes in BMD among the various peak impact energies of the

orbital floor (n=6). A value of $p < 0.05$ was considered statistically significant. Data are presented as means \pm standard deviation (SD).

Four fresh-frozen cadaveric heads were omitted from analysis due to a lack of globes (n=2) or the presence of enophthalmos and facial fracture development (n=2).

Chapter 4

4 Results

4.1 Preliminary Study

Preliminary study results indicated that the energy required to fracture the medial wall of the orbit was greater than that required to fracture the orbital floor. The energy required to induce a fracture of the orbital floor was found to be 6.64 J (drop height of 0.50 m), and the energy required to induce a fracture of the medial orbital wall was found to be ≥ 6.64 J.

4.2 Actual Study

4.2.1 Fracture Pattern Distribution

Sixteen orbits in eight fresh-frozen cadaveric heads were subjected to testing procedures. Two heads were excluded from testing due to a lack of globes.

Not all orbits sustained a fracture. One head (1894) showed a fracture of both the medial orbital and orbital floor after one round of impact. Three heads (1904, 1908, and 1948) showed a fracture on both regions after two rounds of impact. Two heads (1869 and 1906) showed a fracture on both regions after three rounds of impact. Two heads (1864 and 1883) did not sustain any fractures after three rounds of impact (Table 2).

Table 2. Analysis of fracture pattern distribution of cadaveric heads following each round of impact during testing. Eight out of ten fresh-frozen cadaveric heads were tested to compare the fracture threshold on operated vs. non-operated control. Fractures of both the medial wall and orbital floor were seen after one round of impact (n=1), two rounds of impact (n=3), three rounds of impact (n=2), or not at all (n=2).

Cadaveric Head	Height of Impact (m)					
	0.46		0.50		0.56	
	Medial Wall	Orbital Floor	Medial Wall	Orbital Floor	Medial Wall	Orbital Floor
1864	x	x	x	x	x	x
1869	✓	x	✓	x	✓	✓
1883	x	x	x	x	x	x
1894	✓	✓				
1904	✓	x	✓	✓		
1906	x	✓	x	✓	✓	✓
1908	✓	x	✓	✓		
1948	✓	x	✓	✓		

While analyzing the fracture pattern distribution following the completion of all testing procedures, a Fischer's exact test was performed to demonstrate a significant difference in fracture pattern ($p < 0.01$). According to Figure 13, all heads obtained a medial wall fracture on the surgical side and an orbital floor fracture on the non-surgical side (Figure 12).

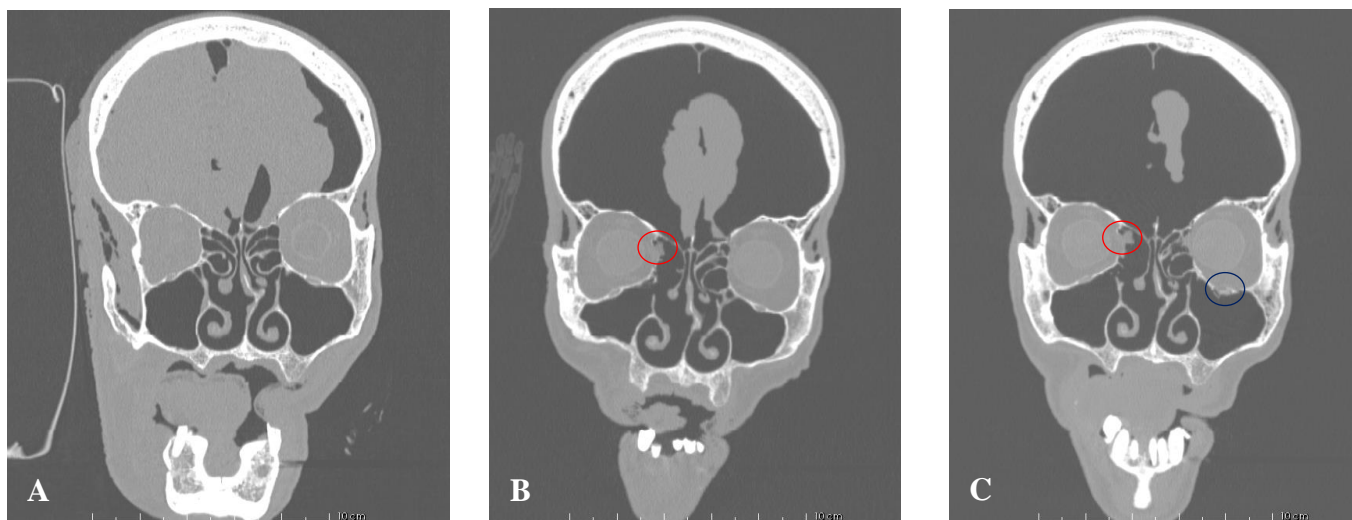


Figure 12. (A) Pre-surgical CT scan of specimen 1869. (B) Medial orbital wall fracture (red) seen on the surgical side post-surgery. (C) Orbital floor fracture (blue) seen on the non-surgical side post-surgery, along with medial orbital wall fracture (red) on surgical side.

Two heads (1864 and 1883) were excluded from analysis due to the fact that they did not acquire any fractures, and were presenting with signs of enophthalmos and facial fracture development. These heads were determined to be outliers in the study.

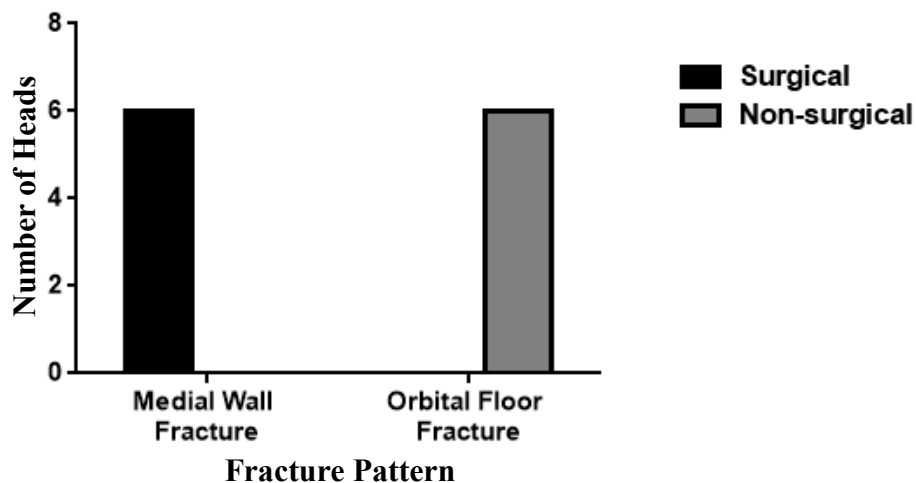


Figure 13. Analysis of fracture pattern distribution of cadaveric heads following testing. Heads (n=6) were impacted on both the surgical and non-surgical sides with all heads acquiring a medial wall fracture on the surgical side and an orbital floor fracture on the non-surgical side. Fisher's exact test ($p < 0.01$).

4.2.2 Impact Energies

Energy delivered by the impact device was calculated using the following equation: $U = mgh$. Drop heights ranged from 0.46 m to 0.56 m, and impact energies ranged from 6.12 J to 7.44 J, respectively.

The peak impact energies required to induce an orbital fracture on the surgical and non-surgical sides, for both the medial orbital wall and orbital floor, are shown in Table 3. All heads (n=5) showed a medial orbital wall impact energy threshold of 6.12 J on the surgical side, except head 1906, which showed a threshold of 7.44 J. Impact energy thresholds varied for the non-surgical side. Two heads (1894 and 1906) showed an orbital floor impact energy threshold of 6.12 J, three heads (1904, 1908, and 1948) showed a threshold of 6.64 J, and one head (1869) showed a threshold of 7.44 J. Comparatively, the energy of a punch is known to be in the range of 100 to 450 J.

All heads sustained a fracture of the medial orbital wall first, followed by a fracture of the orbital floor, with the exception of head 1906, which sustained a fracture of the orbital floor (6.12 J) before the medial orbital wall (7.44 J). Head 1894 sustained a fracture of both the medial orbital wall and the orbital floor after one round of impact (6.12 J). Heads 1864 and 1883 were excluded from analysis.

Table 3. Peak energies required to induce an orbital fracture on the surgical and non-surgical sides, with the associated fracture pattern, for each cadaveric head.

Cadaver Head	Experimental (Surgical) Side			Control (Non-surgical) Side		
	Impact Energy (J)	Medial Wall	Orbital Floor	Impact Energy (J)	Medial Wall	Orbital Floor
1869	6.12	✓	✗	7.44	✗	✓
1894	6.12	✓	✗	6.12	✗	✓
1904	6.12	✓	✗	6.64	✗	✓
1906	7.44	✓	✗	6.12	✗	✓
1908	6.12	✓	✗	6.64	✗	✓
1948	6.12	✓	✗	6.64	✗	✓

Statistical analysis of the impact energies showed that there was no significant difference ($p > 0.05$) in the energies required to induce a fracture of the medial orbital wall on the surgical side and the orbital floor on the non-surgical side (Figure 14).

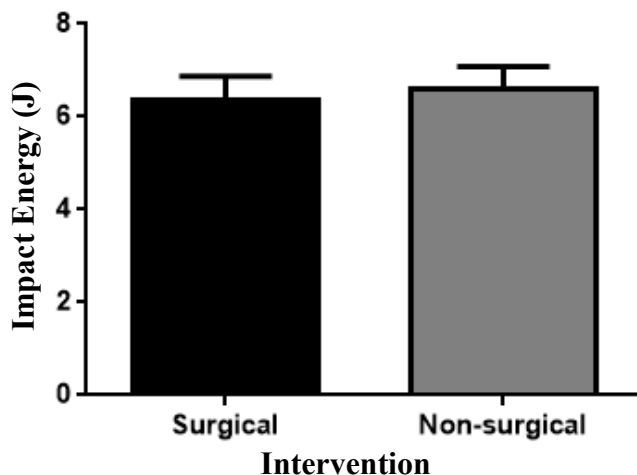


Figure 14. Analysis of impact energies inducing post-surgery fractures. The peak impact energies required to induce orbital fractures were analyzed using GraphPad Prism 6 (surgical, $n=6$; non-surgical, $n=6$). The increase in energy required to induce a fracture on the non-surgical side was not significant (paired two tailed t-test; $p > 0.05$). Data are presented as mean \pm SD.

4.2.3 Bone Mineral Density

Average ρ_{APP} values, calculated for fresh-frozen cadaveric heads ($n=6$), are listed in Table 4.

Table 4. Average ρ_{APP} values, calculated using Materialise Mimics® and LabVIEW System Design Software, for each cadaveric head and associated fracture site via pre-surgical scans.

Cadaver Head	Average Apparent Density (g/cm^3)	
	Medial Wall	Orbital Floor
1864	0.4889971	0.5763782
1869	0.4551908	0.3732463
1883	0.5955582	0.5024309
1894	0.4351643	0.3917295
1904	0.4440026	0.3402720
1906	0.4399272	0.4879000
1908	0.5469874	0.4748342
1948	0.3439292	0.5065735

Statistical analysis of the changes in BMD among the peak impact energies of the medial orbital wall, as well as the orbital floor, showed that there was no significant difference ($p > 0.05$) between various energy values. These results are displayed in Figure 15.

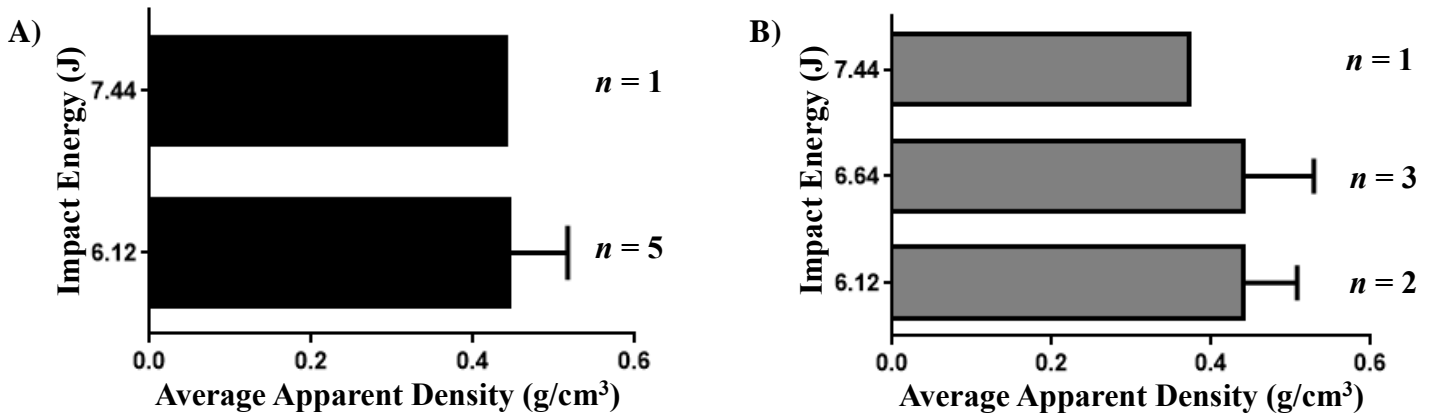


Figure 15. Changes in BMD among various impact energies. **A)** Changes in BMD among the impact energies for the medial orbital wall on the surgical side (unpaired two tailed t-test; $p > 0.05$). **B)** Changes in BMD among impact energies for the orbital floor on the non-surgical side (one-way ANOVA; $p > 0.05$). Data were analyzed using GraphPad Prism 6 and are presented as mean \pm SD.

4.2.4 Summary of Results

All heads presented with a medial wall fracture on the surgical side and orbital floor fracture on the non-surgical side. Results show a trend of reduction in the energy required to induce a fracture in the medial orbital wall post-surgery, compared to the orbital floor, however the reduction was not significant. The change in BMD among the various impact energies for each fracture site was not significant.

Chapter 5

5 Discussion

5.1 Interpretation of Results

This study aimed to assess whether there would be a greater likelihood of the medial orbital wall fracturing, compared to the orbital floor, following FESS. The first objective was to evaluate the occurrence and pattern of post-surgery fractures via CT scanning. According to the results of this study, all heads presented with a medial orbital wall fracture on the surgical side and an orbital floor fracture on the non-surgical side. Overall, the medial orbital wall fractured on the surgical side prior to the fracture of the orbital floor on the non-surgical side.

The second objective was to compare the energy required to induce a fracture in the medial orbital wall, versus the orbital floor, post-surgery. The results showed a trend in the reduction of energy required to induce a fracture in the medial orbital wall, compared to the orbital floor post-surgery.

These results are in accordance with our hypothesis, which predicted an increasing frequency of medial orbital wall fractures post-surgery, as well as a reduction in the energy required to induce a fracture of the medial orbital wall compared to the orbital floor.

5.2 Anatomical Significance

Due to its position and fragility, the orbit tends to be particularly susceptible to fractures (Gosau et al., 2011). The orbital floor and medial orbital wall have a greater likelihood of incurring a fracture, compared to other walls of the orbit. The medial orbital wall is the thinnest wall of the orbit (Braffman et al., 1997). The orbital floor is weakened by the presence of the inferior orbital canal through which the infraorbital vessels and nerve pass through (Bell & Al-Bustani, 2012), and it is located just above the maxillary sinus, which is the largest of the four paranasal sinuses. Previous studies have shown that the sinuses also act as a 'crumple zone' protecting the eye during maxillofacial trauma. As a traumatic force is applied to the eye, hydraulic pressure is transmitted through the globe and an orbital blowout fracture occurs, preventing globe rupture

(Kellman & Schmidt, 2009). The lateral wall and roof of the orbit tend to be less susceptible due to their increased thickness and bone strength (Braffman et al., 1997).

Of the two main fracture mechanisms previously described, the hydraulic mechanism was used to carry out the testing procedures for this study. The hydraulic theory states that hydraulic pressure from the globe is transmitted to the bony orbit, resulting in a fracture of the orbital floor. Although both the buckling and hydraulic mechanisms produce orbital blowout fractures, they present with slightly different characteristics. The buckling mechanism tends to produce smaller, linear fractures along the anterior orbital floor. In contrast, the hydraulic mechanism tends to produce larger, more posterior fractures of both the orbital floor and medial orbital wall (Gart & Gosain, 2014). Previous studies have shown that the hydraulic theory induces trauma to the globe that is dispersed throughout the orbit, resulting in orbital floor fractures and, in some cases, the medial wall as well depending on the amount of energy transmitted (Kellman & Schmidt, 2009). Because the purpose of this study was to compare the skeletal strength of the orbital floor with that of the medial orbital wall, the hydraulic mechanism was chosen.

Preliminary study results showed that the energy required to fracture the medial orbital wall (≥ 6.64 J; drop height of 0.50 m) was greater than that required to fracture the orbital floor (6.64 J). As a result of these values, we decided to test in the range of 0.46 m and 0.56 m. We were able to detect fractures of both the medial orbital wall and orbital floor within this range. Although these values are in line with those published in the literature, they are higher than the minimum threshold values known to induce fractures of the medial orbital wall (≥ 4.90 J) and orbital floor (≥ 2.08 J) (Rhee et al., 2002; Green et al., 1990). However, in addition to the minimum threshold values, Rhee *et al.* (2002) also found that bony displacement, with herniation of orbital contents, was obtained only at heights above 0.50 m (4.9 J), and fractures of the orbital floor were obtained at lower heights with medial wall fractures occurring concomitantly at higher energies (≥ 6.86 J). These results are more in line with the values we have achieved. Furthermore, the higher impact energies found in our study may be due to the difference in cadaveric models used for the preliminary study (fixed) and subsequent studies (fresh-frozen), and the difference in preservation of these models which could ultimately affect their composition.

Results pertaining to the fracture pattern post-surgery, after the completion of testing, showed that the medial orbital wall tended to fracture prior to the orbital floor, except one head (1906) in which the orbital floor fractured prior to the medial orbital wall (Table 2). It was also shown that all medial wall fractures occurred on the surgical side for each cadaveric head, and all orbital floor fractures occurred on the non-surgical side. This difference was statistically significant (Figure 13). The reasoning behind the exception seen in head 1906 is not known. It may simply have been due to a small testing error, such as improper positioning of the head within the testing apparatus. It may also have been due to an inability to detect a fracture in the medial orbital wall with the naked eye, especially if a microfracture had occurred after the first round of impact which could not be identified on the CT scan.

The test results are consistent with our hypothesis. We predicted that the medial wall would be more likely to fracture after having undergone FESS. For the purposes of this study, the procedures performed in FESS included an uncinectomy, maxillary antrostomy, and anterior/posterior ethmoidectomy. Uncinectomy involves removal of the uncinete process, which has an attachment on the lamina papyracea (70%) (Srivastava & Tyagi, 2015; Tuli et al., 2013). The uncinete process, along with the ethmoid air cell septations, may be acting as buttresses for the medial orbital wall. Therefore, removal of these structures during surgery may weaken the medial orbital wall and increase the likelihood of post-surgical fractures in the immediate period following surgery.

This may also explain the decrease in energy required to induce a fracture in the medial orbital wall, compared to the orbital floor, following surgery. Normally, the orbital floor is more likely to fracture than the medial orbital wall (Brown et al., 1999; Hwang et al., 2009). Due to the intervention of FESS, however, and removal of structures which may be supporting this bony region, we saw a reversed trend. Although the difference in impact energies between the two fracture sites was not significant (Figure 14), the trend we saw may have some important clinical implications. Due to the fact that we were working with such a small sample size ($n=6$) when performing statistical analyses, this may be contributed to the lack of a significant difference. Additionally, the impact energy values that resulted from our study ranged from 6.12 J to 7.44 J (Table 3). These values are higher than the minimum threshold values publishes in previous literature and this is because the impact device that we used was heavier, which contributed to an

increased energy value and caused the difference in impact energies to be extremely small. However, our increased energy range also displays a weakness of the study in that we do not know what the actual threshold values were at which the heads could have obtained fractures. This prevents us from being able to make a quantitative comparison between the impact energy values producing fractures in the medial orbital wall and the orbital floor. Although, we are still able to discuss the trend we see with respect to the difference in fracture pattern, as well as occurrence, which fulfils the first objective of this study.

There were two heads in the study which did not present with any fractures and were excluded from statistical analyses: 1864 and 1883. Unlike the other specimens, 1864 and 1883 did not obtain any fractures after three rounds of testing (Table 2). We then subjected these heads to two more impact rounds from heights of 0.60 m and 0.66 m (7.98 J and 8.78 J, respectively). After these two additional rounds, we still did not see any fractures. Furthermore, we noticed that these heads were starting to develop signs of enophthalmos and facial fractures around the orbital region which could have compromised the skeletal structure of the orbit. Therefore, these heads were no longer included in the overall data analysis and were considered to be outliers in the study. The reasoning behind why these heads did not present with fractures is not known. We had several possible theories in mind. One being improper positioning within the testing apparatus. Although positioning the nose of the impact device over the globe allowed for accurate targeting of the weight to the impact point, there may have been slight variances in the position of the impact point once the mass was dropped. A second theory has to do with the bony structure of the orbit in these specimens. We noticed that both 1864 and 1883 had comparatively larger orbits which were also quite sunken. This may have prevented the nose of the impact device from contacting the target site, due to the outer rim of the device being halted by the rim of the orbit, thereby resulting in a lack of fractures. Finally, there may be an increase in bone strength in these individuals, thereby increasing the threshold of energy required to induce fractures. Taking a look at the average ρ_{APP} values for all heads (Table 4), we notice that specimens 1864 and 1883 had higher densities, for both the medial orbital wall and the orbital floor, compared to other specimens.

Bone mineral density is an important element of this study, as it collapses variables that we could not necessarily control for into one measure. These include age, sex, and small sample size.

Furthermore, we do not know whether the specimens we worked with were osteoporotic. Low BMD is considered to be one of the most important determinants of osteoporosis, as well as osteoporotic fractures (Warming, Hassager, & Christiansen, 2002).

When talking about symmetry between the two sides of the face in individuals with pathologies, previous studies have shown that the right side of the face generally tends to be bigger than the left side, however there are no significant differences in the orbit region and minimal differences between the two sides with respect to orbital volume (Rossi, Ribeiro, & Smith, 2003). Therefore, we were safely able to assume for our study that there would be a minimal to no significant difference between the two orbits with respect to bone thickness. While trying to determine whether BMD changed among the various impact energy values for both fracture sites, it was found that there was no significant difference between the values (Figure 15) and this data supports our assumption.

5.3 Clinical Implications

Improved knowledge and recognition of orbital fracture risk following sinus surgery is crucial. Rhinosinusitis is a common condition, the incidence of which continues to rise among adults (Kaplan, 2014). Although medical therapy is the mainstay of therapy among patients with this condition, those with recurrent or chronic rhinosinusitis may be subjected to surgical intervention. In the immediate post-surgery period, patients may be at an increased risk for medial orbital wall fractures. This is implicated in the idea of informed consent. Although the data presented in this study shows that there is no significant difference in the impact energies inducing fractures of the medial orbital wall and orbital floor post-surgery, there is still the trend that the medial orbital wall fractured preferentially over the orbital floor and at lower energy thresholds. Having access to such information may affect the decision of patients who have symptoms of recurrent or chronic sinusitis and are looking to undergo surgery.

5.4 Strengths and Limitations

There are several important strengths to this study. The use of fresh-frozen cadaveric specimens allowed for realistic comparisons of impact energies and fracture detection via CT scans, which could be generalized to the larger population. The use of these specimens also made it possible

for both interventional methods, surgical and non-surgical, to be performed in each specimen. This allowed each head to serve as its own control. If a cadaveric model were not used, only one of the two intervention techniques could have been performed in each head, requiring twice as many subjects to obtain the same results. Another strength of this study is the results that were achieved, which were consistent and expected. There was zero variance in the data with respect to fracture pattern and, although the difference in impact energies between the medial orbital wall and orbital floor was not significant, it was a difference nonetheless and this was in accordance with our predictions. Finally, this study is the first to look at the effect of sinus surgery on orbital fracture risk and assess the implications this may have with respect to patients who have rhinosinusitis.

This study also had some limitations which must be addressed. The first is the sample size of 14 cadaveric heads. This relatively small sample size limits the robustness of the findings. Furthermore, four of these heads were fixed specimens used to conduct the preliminary study, which leaves ten fresh-frozen specimens for the actual study. Although the properties of fresh cadaveric tissue are more indicative of live tissue, only six of the ten fresh cadaveric heads were available for data analysis. Another limitation is that this study was carried out over a span of several months. Working with fresh-frozen specimens involves having to ensure that they are thawed well ahead of time to perform all testing procedures, and frozen again when not in use. This results in multiple freeze-thaw cycles which could have affected the composition of these specimens. In addition, the nature of this study limited the ability to prevent multiple impacts on the same orbits in order to detect fractures. This may have resulted in reduced fracture thresholds from what might have been the actual peak impact values. Finally, this study data may have been limited by human error with respect to all the testing procedures carried out, as well as the CT scans that were read for fracture detection.

5.5 Future Directions

The main priority of future investigations similar to this one should be access to a greater number of specimens. Increasing the sample size would increase the robustness and validity of the findings. This is especially true for fresh-frozen specimens, since they are more comparable to the state of the orbit and its structural composition in a live patient. If more fresh specimens were involved in this study, it would likely be possible to detect a significant difference in the impact

energies that induce a fracture of the medial orbital wall compared to the orbital floor. Moreover, further evaluating the association of BMD with orbital fractures may produce significant results with a larger sample size. This could be important, considering two heads in our study did not present with any fractures after multiple rounds of testing and were calculated to have higher density values for both fracture sites, in comparison to other heads. It may also be useful to test and see which type of fracture is more likely to occur with a specific type of sinus surgery procedure. For the purposes of this study, we performed an uncinectomy with a concurrent maxillary antrostomy and anterior/posterior ethmoidectomy. After these procedures were completed on our specimens, we found that the medial orbital wall was more likely to fracture than the orbital floor overall. Knowledge of the susceptibility of fractures with respect to individual sinus surgery procedures may affect the overall outcome of a study such as this one, as there may be a change in the skeletal composition of specific orbital contents which may alter the formation of other intimately related structures in the region. Furthermore, it may be helpful to assess the variations in uncinete process attachment and the resulting effect on medial orbital wall fractures. With differences in attachment, there may be a change in the susceptibility and fracture pattern of the medial orbital wall, compared to the orbital floor. Finally, this study allows us to evaluate whether sinus surgery conveys an immediate risk with respect to orbital fractures. We do not, however, know whether there is strength that would prevent a medial orbital wall fracture with healing in the long term. Knowing the effects of surgery in the long term would also serve clinical implications for the patient population with respect to informed consent.

5.6 Conclusion

With the increasing incidence of rhinosinusitis comes the increasing risk of patients who may develop recurrent or chronic symptoms. In such cases, if medical therapy fails, surgery may be required. Patients undergoing FESS may be at an increased risk for medial orbital wall fractures as a result of removal of the uncinete process and ethmoid bulla, as well skeletonization of the lamina papyracea. This study demonstrates that i) the medial orbital wall fractures preferentially over the orbital floor post-FESS, ii) all heads presented with a medial orbital wall fracture on the surgical side and orbital floor fracture on the non-surgical side, and iii) there is a trend of reduction in the energy required to induce a fracture in the medial orbital wall post-surgery,

compared to the orbital floor. In addition to the anatomical significance of these results, which show that the uncinat process and ethmoid air cell septations may be acting as buttresses for the medial orbital wall and thereby reducing the energy required to induce fractures, there are clinical implications associated as well with respect to the patient population and informed consent.

Bibliography

1. Gart, M. S., & Gosain, A. K. (2014). Evidence-Based Medicine. *Plastic and Reconstructive Surgery*, 134(6), 1345–1355.
2. Braffman, B. H., Naidich, T. P., & Chaneles, M. (1997). Imaging anatomy of the normal orbit. *Seminars in Ultrasound CT and MRI*, 18(6), 403–412.
3. Morris, D. E., Liliav, B., & Cohen, M. N. (2014). Transcaruncular Approach to the Isolated Medial Orbital Wall Fracture. *Journal of Craniofacial Surgery*, 25(3), 1047–1049.
4. Moore, K.L., Dalley, A.F., & Agur, A.M.R. (2013). *Clinically Oriented Anatomy* (7th ed.). Baltimore: Lippincott, Williams, & Wilkins.
5. Galil, K. (2004). Retrieved March 27, 2016, from <http://www.drgalil.ca/skull/index.htm>
6. Brown, M. S., Ky, W., & Lisman, R. D. (1999). Concomitant ocular injuries with orbital fractures. *The Journal of Cranio-Maxillofacial Trauma*, 5(3), 41–6.
7. Hwang, K., You, S. H., & Sohn, I. A. (2009). Analysis of Orbital Bone Fractures. *Journal of Craniofacial Surgery*, 20(4), 1218–1223.
8. Ellis, E., El-Attar, A., & Moos, K. F. (1985). An analysis of 2,067 cases of zygomatico-orbital fracture. *Journal of Oral and Maxillofacial Surgery : Official Journal of the American Association of Oral and Maxillofacial Surgeons*, 43(6), 417–428.
9. Gosau, M., Schöneich, M., Draenert, F. G., Ettl, T., Driemel, O., & Reichert, T. E. (2011). Retrospective analysis of orbital floor fractures-complications, outcome, and review of literature. *Clinical Oral Investigations*, 15(3), 305–313.
10. Birkenfeld, F., Steiner, M., Becker, M. E., Kern, M., Wiltfang, J., Lucius, R., & Becker, S. T. (2012). Forces charging the orbital floor after orbital trauma. *The Journal of Craniofacial Surgery*, 23(4), 953–6.
11. Ahmad, F., Kirkpatrick, W. N. A., Lyne, J., Urdang, M., Garey, L. J., & Waterhouse, N. (2003). Strain gauge biomechanical evaluation of forces in orbital floor fractures. *British Journal of Plastic Surgery*, 56(1), 3–9.
12. Burm, J.S., Chung, C.H., & Oh, S.J. (1999). Pure orbital blowout fracture: new concepts and importance of medial orbital blowout fracture. *Plastic and Reconstructive Surgery*, 103(7), 1839-1849.
13. Yeo, N.-K., & Kim, E. H. (2015). A Case of Aggravated Medial Orbital Wall Fracture After Reduction of Orbital Floor Fracture. *Journal of Craniofacial Surgery*, 26(8), e691–e693.

14. Jank, S., Schuchter, B., Emshoff, R., Strobl, H., Koehler, J., Nicasi, A., ... Baldissera, I. (2003). Clinical signs of orbital wall fractures as a function of anatomic location. *Oral Surgery, Oral Medicine, Oral Pathology, Oral Radiology, and Endodontics*, 96(2), 149–153.
15. Rhee J. S., Kilde J., Yoganadan N., & Pintar F. (2002). Orbital blowout fractures: experimental evidence for the pure hydraulic theory. *Archives of Facial Plastic Surgery*, 4(2), 98–101.
16. Warwar, R. E., Bullock, J. D., Ballal, D. R., & Ballal, R. D. (2000). Mechanisms of orbital floor fractures: a clinical, experimental, and theoretical study. *Ophthalmic Plastic and Reconstructive Surgery*, 16(3), 188–200.
17. Erling, B. F., Iliff, N., Robertson, B., & Manson, P. N. (1999). Footprints of the globe: A practical look at the mechanism of orbital blowout fractures, with a revisit to the work of Raymond Pfeiffer. *Plastic and Reconstructive Surgery*, 103(4), 1313-1316.
18. Cruz, A. A. V., & Eichenberger, G. C. D. (2004). Epidemiology and management of orbital fractures. *Current Opinion in Ophthalmology*, 15(5), 416–21.
19. Pausch, N. C., Sirintawat, N., Wagner, R., Halama, D., & Dhanuthai, K. (2016). Lower eyelid complications associated with transconjunctival versus subciliary approaches to orbital floor fractures. *Oral and Maxillofacial Surgery*, 20(1), 51-55.
20. Oh, J., Rah, S., & Kim, Y. (2003). Transcaruncular approach to blowout fractures of the medial orbital wall. *Korean Journal of Ophthalmology*, 17, 50-54.
21. Hamdy, R. C. (2016). Bone Mineral Density and Fractures. *Journal of Clinical Densitometry*, 19(2), 125–126.
22. Winzenberg, T. (2011). Dual energy X-ray absorptiometry, 40(1), 43–45.
23. Adams, J. E. (2009). Quantitative computed tomography. *European Journal of Radiology*, 71(3), 415–424.
24. Reeves, J., Knowles, N., Ferreira, L., Athwal, G., & Johnson, J. (2016). Post-hoc calibration methods for quantitative computed tomography. *Unpublished*.
25. Srivastava, M., & Tyagi, S. (2015). Role of Anatomic variations of Uncinate Process in Frontal Sinusitis. *Indian Journal of Otolaryngology and Head & Neck Surgery*.
26. Lund, V. J., Stammberger, H., Fokkens, W. J., Beale, T., Bernal-Sprekelsen, M., Eloy, P., ... Welge-Luessen, A. (2014). European position paper on the anatomical terminology of the internal nose and paranasal sinuses. *Rhinology. Supplement*, (24), 1–34.

27. Tuli, I. P., Sengupta, S., Munjal, S., Kesari, S. P., & Chakraborty, S. (2013). Anatomical Variations of Uncinate Process Observed in Chronic Sinusitis. *Indian Journal of Otolaryngology and Head and Neck Surgery*, 65(2), 157–161.
28. Gnanavelraja, C., Senthilnathan, V., Vijayakumar, M., Ramesh, M., Rajajeyakumar, M., P, T. K. S., & Ismail, M. (2014). Anatomical variations in the superior attachment of uncinat process and its association with frontal sinusitis. *International Medical Journal*, 1(8), 399–401.
29. Pullen, R. L. (2010). Assessing the paranasal sinuses. *Nursing*, 40(5), 49–50.
30. Kaplan, A. (2013). Clinical Summary. *Canadian Family Physician Médecin de Famille Canadien*, 59, 1275-1281.
31. Kaplan, A. (2014). Canadian guidelines for acute bacterial rhinosinusitis: clinical summary. *Canadian Family Physician Médecin de Famille Canadien*, 60(3), 227–34.
32. Damm, M., Quante, G., Jungehueling, M., & Stennert, E. (2002). Impact of functional endoscopic sinus surgery on symptoms and quality of life in chronic rhinosinusitis. *The Laryngoscope*, 112(2), 310–315.
33. Orlandi, R. R., Kingdom, T. T., Hwang, P. H., Smith, T. L., Alt, J. A., Baroody, F. M., ... Kennedy, D. W. (2016). International Consensus Statement on Allergy and Rhinology: Rhinosinusitis. *International Forum of Allergy & Rhinology*, 6(S1), S22–S209.
34. Bublik, M., Herman, B., & Younis, R. (2009). Functional endoscopic sinus surgery. *Operative Techniques in Otolaryngology-Head and Neck Surgery*, 20(3), 167–171.
35. Senior, B.A., Kennedy, D.W., Tanabodee, J., Kroger, H., Hassab, M., Lanza, D. (1998). Long-term Results of Functional Endoscopic Sinus Surgery. *The Laryngoscope*, 108(2), 151-157.
36. McMains, K. C. (2008). Safety in endoscopic sinus surgery. *Current Opinion in Otolaryngology & Head and Neck Surgery*, 16(3), 247–251.
37. Krings, J. G., Kallogjeri, D., Wineland, A., Nepple, K. G., Piccirillo, J. F., & Getz, A. E. (2014). Complications of primary and revision functional endoscopic sinus surgery for chronic rhinosinusitis. *Laryngoscope*, 124(4), 838–845.
38. Wormald, P.J., van Renen, G., Perks, J., Jones, J.A., Langton-Hewer, C.D. (2005). The effect of the total intravenous anesthesia compared with inhalational anesthesia on the surgical field during endoscopic sinus surgery. *American Journal of Rhinology*, 19(5), 514-520.

39. Singhanian, A. A., Bansal, C., Chauhan, N., & Soni, S. (2012). A Comparative Study of Two Different Uncinectomy Techniques : Swing-Door and Classical, *24*(2), 63–67.
40. Kellman, R. M., & Schmidt, C. (2009). The paranasal sinuses as a protective crumple zone for the orbit. *Laryngoscope*, *119*(9), 1682–1690.
41. Green, R. P., Peters, D. R., Shore, J. W., Fanton, J. W., & Davis, H. (1990). Force necessary to fracture the orbital floor. *Ophthalmic Plastic and Reconstructive Surgery*, *6*(3), 211-217.
42. Bell, R. B., & Al-Bustani, S. S. (2012). Orbital Fractures. *Current Therapy In Oral and Maxillofacial Surgery*, *4*(3), 304–323.
43. Warming, L., Hassager, C., & Christiansen, C. (2002). Changes in bone mineral density with age in men and women: A longitudinal study. *Osteoporosis International*, *13*(2), 105–112.
44. Rossi, M., Ribeiro, E., & Smith, R. (2003). Craniofacial asymmetry in development: An anatomical study. *Angle Orthodontist*, *73*(4), 381–385.

Appendix A: Rights and Permissions

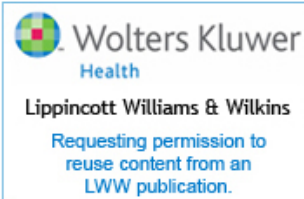


RightsLink®

Home

Create Account

Help



Book: Clinically Oriented Anatomy
Author: Keith L Moore, Anne M. R. Agur,
Publisher: Wolters Kluwer Health
Date: 2013
 Copyright © 2013, Lippincott Williams

LOGIN

If you're a **copyright.com** user, you can login to RightsLink using your copyright.com credentials. Already a **RightsLink** user or want to [learn more?](#)

Dissertation/Thesis Reuse

LWW grants permission for a maximum of 3 figures or tables without charge, provided that the material is for limited dissertation/thesis distribution. If you are required to post your dissertation/thesis on the university website/intranet/library reserve, access to it must be password-protected. Should you wish to publish your paper in the future, you will need to reapply for permission to use our material.

BACK

CLOSE WINDOW

Copyright © 2016 [Copyright Clearance Center, Inc.](#) All Rights Reserved. [Privacy statement.](#) [Terms and Conditions.](#)

Comments? We would like to hear from you. E-mail us at customercare@copyright.com

Appendix B: Permissions to Scholarship@Western

I grant, on behalf of UWO, the non-exclusive right to distribute my submission publicly as part of the University of Western Ontario Institutional Repository *Scholarship@Western*.

Curriculum Vitae

Name: Rootu Joshi

Post-secondary Education and Degrees: The University of Western Ontario
London, Ontario, Canada
BSc Honors Specialization in Medical Sciences
2010-2014

The University of Western Ontario
London, Ontario, Canada
MSc Clinical Anatomy
2014-2016

Honours and Awards: AAA Travel Award
2016

Western Graduate Research Scholarship
2014-2016

Related Work Experience Teaching Assistant
The University of Western Ontario
2014-2016

- Systemic Human Anatomy 3319
- Inflammation in Diseases 4200
- Medical Imaging for Clinical Anatomy 9567L
- Gross Anatomy for Dentistry
- Gross Anatomy for Medicine (Year 1 and 2)

Professional Development:

Certificate in University Teaching and Learning April 2016
Western Teaching Support Center

- **Continuing Professional Development** February 2015
 - Designing Your Teaching Roadmap
 - Protecting Your Digital Self
- **Winter Conference on Teaching** January 2015
- **Future Professor Workshop Series** October 2014 to November 2015
 - Putting Together a Teaching Dossier
 - Writing a Teaching Philosophy Statement
 - Active Learning: Beyond Lab Skills

- Marking & Effective Feedback
 - Winter Conference on Teaching
 - So You Think You're a Fraud? Overcoming Imposter Syndrome
 - Critical Thinking in the Information Age: Helping Undergrads Find & Evaluate Scientific Information
 - Education for Global Citizenship
- **Research Ethics Module** October 2014
 - Introduction to the 2nd edition of the Tri-Council Policy Statement: Ethical Conduct for Research Involving Humans (TCPS 2)
 - **TA Day: Graduate Student Conference on Teaching** September 2014

Research Poster Presentations:

Joshi R, Johnson M, Willmore K, Galil K, Jenkyn T, Sowerby L, Moore C. (2015). Does Sinus Surgery Increase the Risk of Orbital Fractures in Patients?

- Poster Presentation at Schulich Dentistry Annual Research Day, London, Ontario.
- Poster Presentation at the Department of Anatomy and Cell Biology Annual Research Day, London, Ontario.

Joshi R, Johnson M, Willmore K, Galil K, Jenkyn T, Sowerby L, Moore C. (2016). Assessing the Effect of Sinus Surgery on Orbital Fractures: Implications for Patients with Sinusitis.

- Poster Presentation at London Health Research Day, London, Ontario.
- Poster Presentation at the American Association of Anatomists Meeting at Experimental Biology, San Diego, California.

Certifications and Professional Memberships:

Western Certificate in University and Teaching
2016

American Association of Anatomists Graduate Student Member
2015-2016